Theory of action potential wave block at-a-distance in the heart

Niels F. Otani*
Department of Biomedical Sciences, Cornell University, Ithaca, New York 14853, USA
(Received 30 January 2006; revised manuscript received 25 August 2006; published 20 February 2007)

Propagation failure of an action potential wave at a finite distance from its source (so-called type-II block) may cause spiral wave formation or wave breakup in the heart, phenomena that are believed to underlie lethal and nonlethal heart rhythm disorders. In this study, we develop a sufficient condition for this type of block in a homogeneous, spatially one-dimensional system. Using a topological argument, we find that type-II block of a wave will always occur when launched within a finite range of times if the velocity of the trailing edge of the preceding wave, as measured at the stimulus site, is smaller than the velocity of a wave launched with the minimum diastolic interval (DI) for which propagation is possible. This "blocking condition" is robust, remaining valid even when memory and waveback electrotonic effects are included. The condition suggests that type-II block is greatly facilitated when waves are initiated at irregular intervals in time such that (1) the velocities of consecutive waves are as different as possible and (2) the DIs preceding each wave fall on the steeply sloped portion of the action potential duration restitution curve as often as possible. The set of timing intervals between stimuli that are predicted by the blocking condition to produce block are found to be consistent with these guidelines, and also to agree well with a coupled-maps computer simulation model, for the case of waves launched by four rapidly and irregularly timed stimuli.

DOI: 10.1103/PhysRevE.75.021910 PACS number(s): 87.19.Hh, 87.10.+e, 05.45.−a, 87.19.Nn

I. INTRODUCTION

Previous studies have shown that the failure or "block" of a propagating cardiac action potential wave can lead to spiral wave reentry in the heart, a dangerous condition that often results in lethal cardiac rhythms such as ventricular fibrillation (e.g., Witkowski *et al.* [1], Chen *et al.* [2]). Recently, some researchers have focused their attention on block created through the interactions that occur within a closely spaced train of action potential waves as a method for studying this behavior. In one such study, Fox *et al.* [3] showed, in both a Purkinje fiber experiment and an ion channel based mathematical model, that rapid, constant-interval pacing at one end of the fiber can lead to block of some of the resulting action potentials at some distance from the pacing site, a phenomenon known as "type-II" block (to distinguish it from type-I block, which is defined to occur in the immediate vicinity of the stimulation site). An intriguing pattern of action potential wave propagation was observed to develop prior to block in these studies. The pattern was identified as "discordant alternans," that is, alternations in wave morphology from one action potential to the next that are out of phase with one another at different points in space. Pastore *et al.* [4] have also observed discordant alternans in guinea pig ventricular muscle during constant pacing, seeing a "long-short-long-short" pattern of action potential durations (APDs), while a "short-long-short-long" pattern appeared at other locations. The discordant alternans pattern was found to predispose the tissue to the formation of reentrant waves and ventricular fibrillation upon slight acceleration of the pacing frequency. The relationship of discordant alternans to type-II block has led to recent theoretical and computational studies. Watanabe *et al.* [5] developed a mathematical theory for discordant alternans, and demonstrated that tissue heterogeneity is not required for its formation. Echebarria and Karma [6] have constructed a partial differential equation governing the amplitude of alternans in space, and used it to explain several features of discordant alternans, including its wavelength and characteristic length scales.

The phenomenon of alternans, and by implication, subsequent spiral wave breakup and fibrillation, has been linked to the steepness of the slope of the APD restitution function, that is, the function that relates the APD to the immediately preceding diastolic interval (DI). Alternans is readily produced when constant pacing is applied within a mathematical model based on the APD restitution function when the slope of the function is greater than 1 [7,8]. Karma [9] demonstrated that, when the spiral wave rotation period was short enough and the restitution function steep enough, alternans in APD from one rotation of the spiral wave to the next often leads to block of portions of the wave, resulting in spiral wave breakup. A coupled maps simulation described by Fox *et al.* [3] exhibited discordant alternans and subsequent block when portions of the APD restitution function had slope greater than 1. Garfinkel *et al.* [10] have shown that bretylium, an agent that flattens the restitution function, can convert ventricular fibrillation back to ventricular tachycardia in pig hearts. Clayton and Taggart [11] conducted computer simulations showing how a spatial heterogeneity in the restitution function causes the block of a portion of a propagating wave, subsequent reentry, and breakup if the slope is greater than 1. The steepness of the APD restitution function is not, however, by any means the sole determinant of the development of alternans and block; as discussed by Cherry and Fenton [12], electrotonic and short-memory effects are, in general, important as well.

Recently, Fox *et al.* [13] extended these studies by applying simulation techniques directly to the occurrence of type-II block created by a short series of rapid but irregularly timed stimuli. The study again showed a correlation between

*Electronic address: nfo1@cornell.edu

a steep restitution function and the tendency for block to occur. It then went on to determine which combinations of timings of the irregularly spaced stimuli actually resulted in block. Studies of block created through this process may be more clinically relevant, because they serve as models of short runs of rapid rhythm in the heart that often precede the onset of ventricular fibrillation (VF). Computer simulations also have provided evidence that short and irregular timings can develop between successive wavefronts of a rotating spiral wave pattern through a number of different mechanisms, leading to subsequent breakup of the wave [14].

The purpose of the present study is to develop a mathematical theory that sheds light on what factors are important in determining when type-II block occurs in this very important situation of brief, irregular, rapid pacing. The theory provides a general mechanism for block that may be useful for predicting the patterns of premature beats that may be especially dangerous in predisposing the heart tissue to the development of ventricular tachyarrhythmias. The results may also be useful in developing approaches to interrupt or subvert such sequences and thereby prevent arrhythmia initiation. In Sec. II of this paper, we give our assumptions and derive a sufficient condition for type-II block to occur. In Sec. III we show how this blocking condition depends on preceding data and on the APD and conduction velocity restitution functions. Section IV then applies these relationships to the case of short runs of four premature stimuli. In Sec. V, the resulting formula is used to predict which combinations of time intervals among these stimuli will lead to block for a number of different APD restitution functions. The predictions are compared to results from our own coupled-maps computer simulation, and to those of Fox *et al.* [13]. The mechanism by which block occurs is discussed for each case. We then briefly describe in Sec. VI how accounting for so-called "memory" effects modifies our results. A discussion and summary of the results are presented in Sec. VII.

II. CONDITION FOR TYPE-II BLOCK

A. Definitions and assumptions

Our description of the mechanism responsible for type-II action potential propagation block is based on a formalism previously employed by Courtemanche *et al.* [15] to describe propagation of action potential waves in a ring, and also more recently by Watanabe *et al.* [5], Fox *et al.* [16], and Cain *et al.* [17] to a linear one-dimensional (1D) cable. The formalism relies heavily on visualization of the action potentials in *t-x* (time-space) coordinates. Accordingly, a brief discussion of the characteristics of traveling action potential waves, as they appear in *t-x* space, would seem appropriate.

We will be considering propagation in one spatial dimension, x, with action potentials being launched from one end of the system, which we label $x=0$, and propagating in the positive x direction. The motion of the leading edge of the nth wave, which we also refer to as the wavefront, or the depolarization wave, is described by the time, $t_d^n(x)$, that the wavefront passes through various locations x. The wave lasts for a finite time once the wavefront passes. This time is called the action potential duration $[\mathrm{APD}_n(x)]$ and is represented by the vertical width of the action potential region in *t-x* space shown in Fig. 1. Similarly, the locus of points in *t-x* space marking the end of the nth action potential wave together represents the trailing edge of the wave, which we will refer to as the repolarization wave $t_r^n(x)$. (Technically, this locus of points is not really a wave, but it is convenient to think of it as a wave entity here, with a definite propagation velocity, etc.) At each point x in space, after repolarization occurs, a finite time elapses before the $(n+1)$st wave arrives; this time is called the diastolic interval (DI), with duration $\mathrm{DI}_n(x)$. It is represented as the vertical width of the gap between action potentials in Fig. 1.

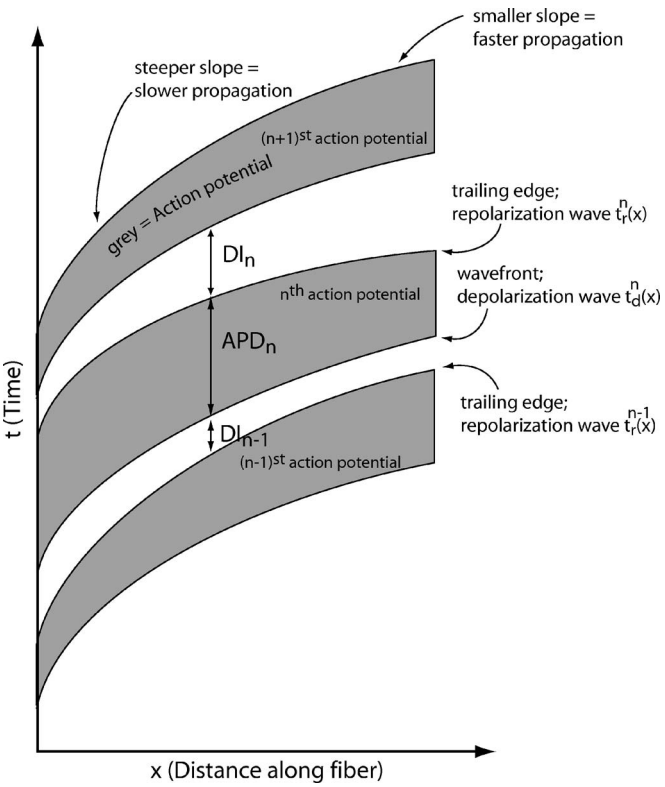

FIG. 1. Characteristics of action potential waves as plotted in *t-x* space.

The speed of the wavefront, or its "conduction velocity" (CV), is just $1/(dt_d^n/dx)$, the inverse of the slope of the nth wavefront as it appears in *t-x* space. Thus the faster a wavefront travels, the flatter is its trajectory. Similarly, the slope of the nth repolarization wave, dt_r^n/dx, is the inverse of the speed of the trailing edge of the wave.

We will make three assumptions in our analysis of this system. First, we assume that the CV of the nth wave at any location x depends on the preceding DI at that location, $\mathrm{DI}_{n-1}(x)$. The wavefront speed is thus given by a function $v[\mathrm{DI}_{n-1}(x)]$, often referred to as the CV restitution function. Second, we will make a similar assumption about the APD, namely, that it is a function of the preceding diastolic interval at the same location x; that is, $\mathrm{APD}_n(x)=a[\mathrm{DI}_{n-1}(x)]$. Here, $a(\mathrm{DI})$ is known as the APD restitution function. Finally, we will assume that propagation failure (action potential block) of the nth wave occurs at a location x when it arrives at that location with diastolic interval $\mathrm{DI}_{n-1}(x)$ less than a specified constant value, which we call $\mathrm{DI}_{\min}$.

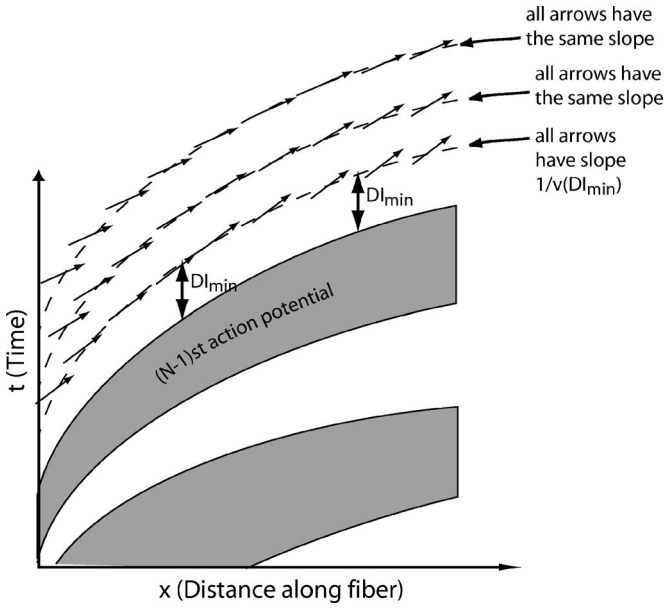

FIG. 2. Orientation of velocity vectors for possible trajectories of the Nth wavefront at different times and locations following the repolarization of the $(N-1)$st wave. Dashed lines are contours of constant $\mathrm{DI}_{N-1}(x)$, including the contour of $\mathrm{DI}_{N-1}(x)=\mathrm{DI}_{\mathrm{min}}$. The slopes of all vectors on a given constant-DI_{N-1} contour are the same (despite an optical illusion that may suggest the contrary), since the slopes are just the inverse velocities, which are in turn functions of DI_{N-1}.

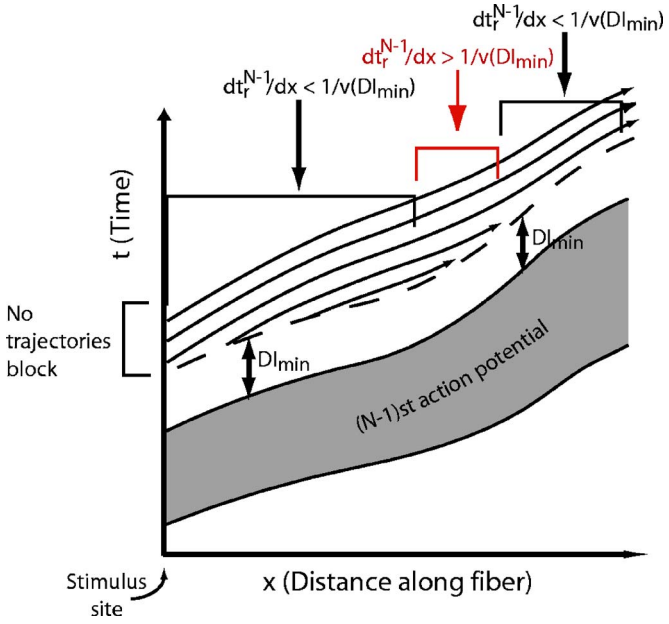

FIG. 3. (Color online) Illustration showing that type-II block can fail to occur even though $dt_r^{N-1}(x)/dx > 1/v(\mathrm{DI}_{\mathrm{min}})$ in a region away from the stimulus site.

B. Local condition for block

We can now characterize in a simple way how a particular wavefront, say, the Nth wavefront, behaves, and potentially blocks, as it follows on the tail of the $(N-1)$st wave. (We will use the index N to refer specifically to the wave that potentially blocks, while n is a generic index referring simply to the nth wave.) The propagation speed of any wavefront passing through a given location x at a given time $\mathrm{DI}_{N-1}(x)$ later than the repolarization time $t_r^{N-1}(x)$ may be denoted by a vector with slope $1/v[\mathrm{DI}_{N-1}(x)]$, as shown in Fig. 2. The trajectory $t_d^N(x)$ of the Nth wavefront must be tangent to these velocity vectors everywhere along its length.

We note that all velocity vectors passing through a curve of constant $\mathrm{DI}_{N-1}(x)$ must by necessity have the same slope. This is, in particular, true for the curve on which $\mathrm{DI}_{N-1}(x)=\mathrm{DI}_{\mathrm{min}}$. The orientation of these vectors relative to the slope of this curve is the key to determining whether action potential block is possible at the corresponding space and time. If the vector points into the region below the curve, the diastolic interval preceding the Nth wavefront will fall below $\mathrm{DI}_{\mathrm{min}}$, immediately extinguishing the wave. All propagation blocks occur in this manner in this system. The velocity vector will be oriented in this way when its slope is less than the slope of the constant $\mathrm{DI}_{N-1}=\mathrm{DI}_{\mathrm{min}}$ curve, as should be clear from Fig. 2. In turn, the slope of this curve is the same as the slope of the repolarization wave at the same location. Thus, when this slope $dt_r^{N-1}(x)/dx$ is greater than the velocity vector slope $1/v(\mathrm{DI}_{\mathrm{min}})$, the action potential wave "runs into" the slower-moving repolarization wave, and block of the action potential wave occurs, as described previously by Qu *et al.* [18]. We will refer to this condition,

$$dt_r^{N-1}(x)/dx > 1/v(\mathrm{DI}_{\mathrm{min}}), \tag{1}$$

as the "blocking condition" for the Nth wave to block at location x.

C. Sufficient condition for block at-a-distance

The existence of segments of the $\mathrm{DI}_{N-1}(x)=\mathrm{DI}_{\mathrm{min}}$ curve where the blocking condition holds does not necessarily mean that the Nth wave launched from the stimulus site at $x=0$ has a chance of blocking. Wave trajectories originating at $x=0$ still must find their way to the segment of the curve on which the condition holds. Such trajectories do not always exist, as illustrated in Fig. 3. Here, a region satisfying the blocking condition exists, but when the trajectories terminating in this region are traced backwards, they are found to originate on the $\mathrm{DI}_{N-1}(x)=\mathrm{DI}_{\mathrm{min}}$ curve, and thus are not generated at the stimulus site. Action potentials actually launched from the stimulus site enter the region where the condition is satisfied with large enough DIs to bypass the region, and thus do not block. This shows that the mere existence of a region satisfying the condition somewhere in the system is not sufficient to guarantee that stimuli launched from a specified location will block.

There is, however, an important case for which type-II wave block is guaranteed. As illustrated in Fig. 4, if the stimulus site itself is included inside one of the segments in which the blocking condition (1) holds, then the existence of a set of trajectories launched from that site that block at some finite distance into the tissue is assured. We can see this from a simple topological argument. If we start from any point along the segment of the curve satisfying the blocking con-

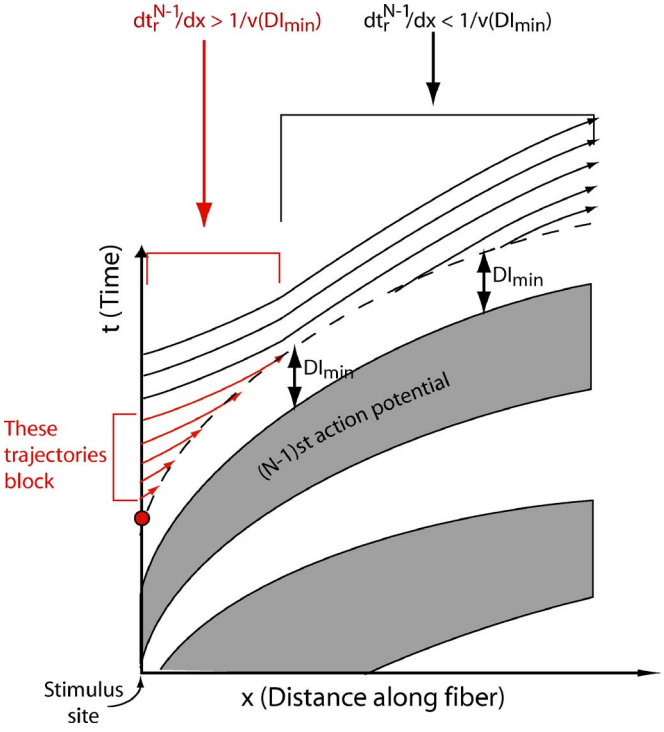

FIG. 4. (Color online) Illustration showing that a certain number of trajectories of the system must exhibit type-II block if $dt_r^{N-1}/dx > 1/v(\mathrm{DI}_{\mathrm{min}})$ at the stimulus site, here located at the left edge of the system.

dition and trace the trajectory (shown in red in Fig. 4) that extinguishes at that point backwards (i.e., to the left in the figure) to its origin, we see that it has no choice but to hit the t axis where $x=0$, implying that it had to have been launched from $x=0$. The trajectories could not have originated from some point on the $\mathrm{DI}_{N-1}(x)=\mathrm{DI}_{\mathrm{min}}$ curve, the only other possibility, because all such points to the left of the point of extinction of the trajectory have their velocity vectors pointing into rather than out of the $\mathrm{DI}_{N-1}<\mathrm{DI}_{\mathrm{min}}$ region.

In turn, a finite segment of the $\mathrm{DI}_{N-1}(x)=\mathrm{DI}_{\mathrm{min}}$ curve around the stimulus site will always satisfy the blocking condition if the stimulus site itself satisfies the condition, as long as $dt_r^{N-1}(x)/dx$ is continuous. We have shown, therefore, that if the repolarization wave of the $(N-1)$st action potential satisfies the blocking condition $dt_r^{N-1}/dx > 1/v(\mathrm{DI}_{\mathrm{min}})$ specifically *at the stimulus location*, then the Nth action potential will always exhibit type-II block if launched with a DI between $\mathrm{DI}_{\mathrm{min}}$ and some larger value.

We note that, while satisfying the blocking condition at the stimulus site is sufficient to yield type-II block, it is not necessary. Figure 5 illustrates the point. We see that it is still possible for block to occur even though the blocking condition is not satisfied at the stimulus site. In this case, action potentials launched at the stimulus site manage to find a distant region where the blocking condition is satisfied.

III. DEPENDENCE OF TYPE-II BLOCK ON ACTION POTENTIAL AND CONDUCTION VELOCITY RESTITUTION

We can determine when the blocking condition will be satisfied at the stimulus site by developing relationships be-

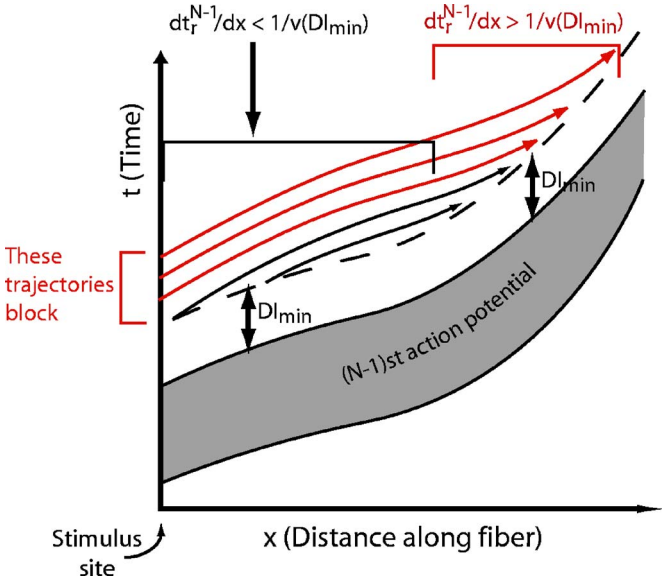

FIG. 5. (Color online) Illustration of how block can still occur even though $dt_r^{N-1}(x)/dx < 1/v(\mathrm{DI}_{\mathrm{min}})$ at the stimulus site.

tween the slope of the repolarization wave dt_r^{N-1}/dx and the slopes of preceding waves. Relationships of this type have been used previously [17–19]. Here we repeat the calculation briefly using a simple geometric argument.

In general, for any series of waves, we can evaluate the relationships between the slopes of the depolarization and repolarization times of the waves by considering the change in these quantities over a small spatial interval Δx. As depicted in the upper portion of Fig. 6, the change in time of repolarization $t_r^n(x)$ of the nth action potential between $x=0$ and $x=\Delta x$ is a convenient measure of the slope t_r^n at $x=0$, being equal to $(dt_r^n/dx)\Delta x$. This change in time is composed of two components.

The first component is the change in time of repolarization of the nth action potential over distance Δx that would have resulted if the APD had not changed over that same distance. If that were the case, then the trailing edge of the nth action potential would have had the same slope as the leading edge, namely, $1/v(\mathrm{DI}_{n-1})$, resulting in a change in time of $[1/v(\mathrm{DI}_{n-1})]\Delta x$, as shown in the figure. The second component is an adjustment to the first that takes into account the fact the APD actually does change over the distance Δx. Mathematically this change may be written as $(d\mathrm{APD}_n/dx)\Delta x$. Consequently, we find that

$$\frac{dt_r^n}{dx} = \frac{1}{v(\mathrm{DI}_{n-1})} + \frac{d\mathrm{APD}_n}{dx}. \tag{2}$$

With an analogous argument, we can see from the lower portion of Fig. 6 that the slope of a given wavefront is also related to the slope of the trailing edge of the preceding wave through the formula

$$\frac{1}{v(\mathrm{DI}_n)} = \frac{dt_r^n}{dx} + \frac{d\mathrm{DI}_n}{dx}, \tag{3}$$

where we have substituted n for $n-1$ in the notation in the figure (possible since the argument applies generally to all propagating waves).

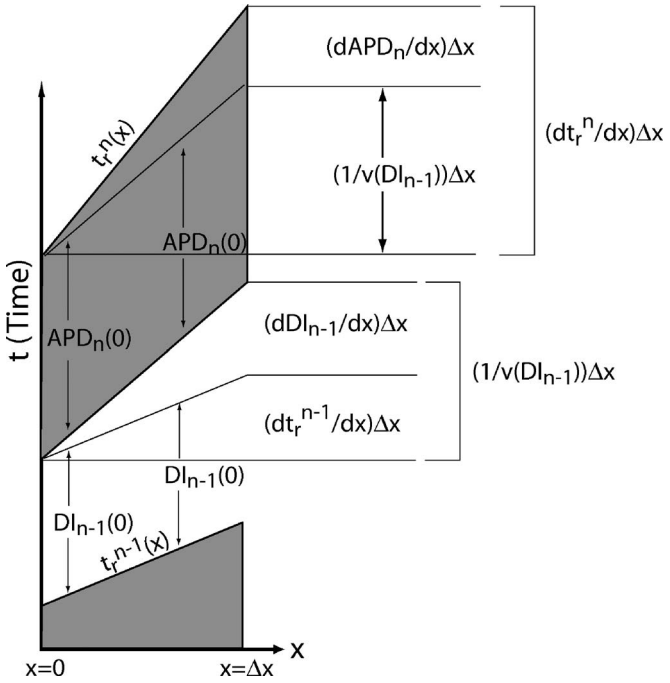

FIG. 6. Geometrical relationship between the wave back slope dt_r^n/dx and wavefront slope $1/v(\mathrm{DI}_{n-1})$ (upper portion of figure), and between the wavefront slope $1/v(\mathrm{DI}_{n-1})$ and the preceding wave back slope dt_r^{n-1}/dx (lower portion) based on the differences in the quantities DI_{n-1} and APD_n evaluated a small distance Δx apart.

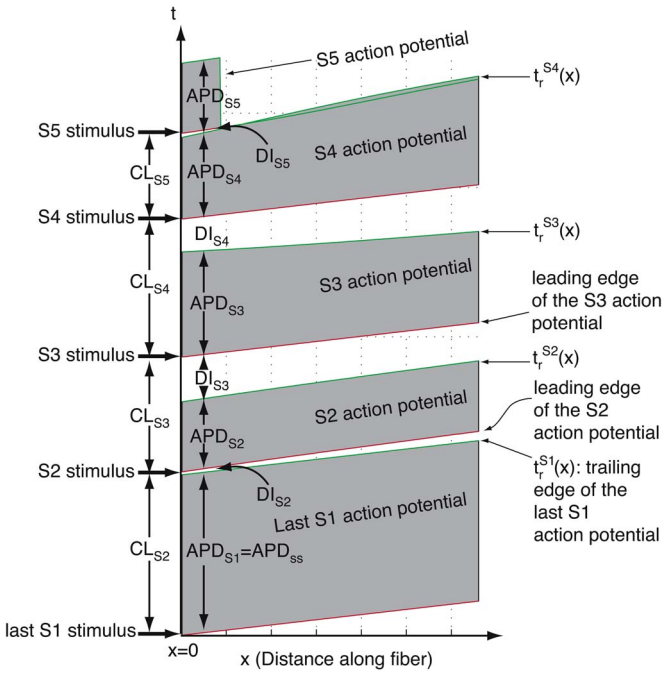

FIG. 7. (Color online) Definitions and space-time relationships among the quantities DI_{S2} through DI_{S5}, $\mathrm{APD}_{S1}=\mathrm{APD}_{SS}$ through APD_{S5}, CL_{S2} through CL_{S5}, the last S1 stimulus, and stimuli S2 through S5, as they appear in x-t space. Also shown are the functions defined for following the leading and trailing edges of selected waves.

By now evaluating Eq. (2) at $n=N-1$, subtracting $1/v(\mathrm{DI}_{\min})$ from both sides and making use of the chain rule, we obtain the following expression:

$$\frac{dt_r^{N-1}}{dx} - \frac{1}{v(\mathrm{DI}_{\min})} = \frac{1}{v(\mathrm{DI}_{N-2})} - \frac{1}{v(\mathrm{DI}_{\min})} + a'(\mathrm{DI}_{N-2})\frac{d\mathrm{DI}_{N-2}}{dx}. \tag{4}$$

When this expression is positive at the stimulus site, the blocking condition is satisfied there, and thus block at-a-distance of the Nth action potential for some range of DIs above $\mathrm{DI}_{\min}$ is assured. Here $a'(\mathrm{DI})$ is the derivative of the APD restitution function with respect to DI.

We find another useful relation by subtracting off $1/v(\mathrm{DI}_n)$ instead of $1/v(\mathrm{DI}_{\min})$ from both sides of Eq. (2). Substituting Eq. (3) we obtain

$$\frac{d\mathrm{DI}_n}{dx} = \frac{1}{v(\mathrm{DI}_n)} - \frac{1}{v(\mathrm{DI}_{n-1})} - a'(\mathrm{DI}_{n-1})\frac{d\mathrm{DI}_{n-1}}{dx}. \tag{5}$$

This equation shows how $d\mathrm{DI}/dx$ is related to its previous value. The relationship is important, because it gives us a means to determine how the last term in Eq. (4) depends on the dynamics of preceding action potential waves.

IV. GENERATION OF TYPE-II BLOCK USING PREMATURE STIMULI

One protocol by which type-II block can be produced is to first apply a series of stimuli (called S1 stimuli) at relatively long, constant intervals, and then follow up with a small number of stimuli (labeled S2,S3,S4,S5,…) applied at shorter, irregular intervals. Here we look specifically at the case in which stimuli up to S5 are applied. The use of other numbers of premature stimuli are, of course, possible. We use the four premature stimuli S2 through S5, a large enough number to give a flavor for what types of dynamics are possible, while small enough to yield manageable calculations. Additionally, the use of these four premature stimuli allows us to make direct comparisons to previous work.

The S1 stimuli are assumed to be applied with an interstimulus interval long enough to avoid the appearance of alternans (that is, the alternation of APD from one stimulus to the next). In the absence of alternans, the train of generated action potential waves settles down to a time-independent (i.e., 1:1) and spatially uniform pattern. Thus, for n large enough, $\mathrm{APD}_n(x)\approx\mathrm{APD}_{SS}$, where APD_{SS} is a constant steady state value. Similarly, $\mathrm{DI}_n(x)$ settles down to a constant value DI_{SS} and the conduction velocity settles down to a steady state velocity $v(\mathrm{DI}_{SS})$.

Once the pattern of action potentials has settled, the first premature stimulus S2 is delivered with a much shorter diastolic interval, $\mathrm{DI}_{S2}\ll\mathrm{DI}_{SS}$. (Note that, here and below, DI_{Sk} for $k=2$ through 5, is the DI *preceding* the S_kth stimulus. See Fig. 7 for definitions.) Applying Eq. (4) to the repolarization wave of the last S1 action potential, we obtain that the blocking condition for block of the S2 action potential is satisfied when

$$\frac{dt_r^{S1}}{dx} - \frac{1}{v(\mathrm{DI}_{\min})} = \frac{1}{v(\mathrm{DI}_{SS})} - \frac{1}{v(\mathrm{DI}_{\min})} \tag{6}$$

is positive at the stimulus site. Here, $t_r^{S1}(x)$ defines the repolarization times of the last S1 action potential wave.

We can derive the blocking condition for S3 through S5 by repeated substitution of Eq. (5) into Eq. (4) evaluated for the repolarization waves of S2 through S4. All quantities are evaluated at the stimulus site. We find that a range of S3 waves will exhibit type-II block when

$$\frac{dt_r^{S2}}{dx} - \frac{1}{v(\mathrm{DI}_{\min})} = \left(\frac{1}{v(\mathrm{DI}_{S2})} - \frac{1}{v(\mathrm{DI}_{\min})}\right) - a'(\mathrm{DI}_{S2})\left(\frac{1}{v(\mathrm{DI}_{SS})} - \frac{1}{v(\mathrm{DI}_{S2})}\right) \tag{7}$$

is positive. Similarly, we find that a range of S4 waves will encounter type-II block when the following quantity is positive:

$$\frac{dt_r^{S3}}{dx} - \frac{1}{v(\mathrm{DI}_{\min})} = \left(\frac{1}{v(\mathrm{DI}_{S3})} - \frac{1}{v(\mathrm{DI}_{\min})}\right) - a'(\mathrm{DI}_{S3})\left(\frac{1}{v(\mathrm{DI}_{S2})} - \frac{1}{v(\mathrm{DI}_{S3})}\right) + a'(\mathrm{DI}_{S3})a'(\mathrm{DI}_{S2})\left(\frac{1}{v(\mathrm{DI}_{SS})} - \frac{1}{v(\mathrm{DI}_{S2})}\right), \tag{8}$$

and that a range of S5 waves will exhibit type-II block when

$$\begin{aligned}\frac{dt_r^{S4}}{dx} - \frac{1}{v(\mathrm{DI}_{\min})} &= \left(\frac{1}{v(\mathrm{DI}_{S4})} - \frac{1}{v(\mathrm{DI}_{\min})}\right) - a'(\mathrm{DI}_{S4})\left(\frac{1}{v(\mathrm{DI}_{S3})} - \frac{1}{v(\mathrm{DI}_{S4})}\right) \\ &\quad + a'(\mathrm{DI}_{S4})a'(\mathrm{DI}_{S3})\left(\frac{1}{v(\mathrm{DI}_{S2})} - \frac{1}{v(\mathrm{DI}_{S3})}\right) \\ &\quad - a'(\mathrm{DI}_{S4})a'(\mathrm{DI}_{S3})a'(\mathrm{DI}_{S2}) \\ &\quad \times\left(\frac{1}{v(\mathrm{DI}_{SS})} - \frac{1}{v(\mathrm{DI}_{S2})}\right) \\ &\equiv b(\mathrm{DI}_{S2},\mathrm{DI}_{S3},\mathrm{DI}_{S4}),\end{aligned} \tag{9}$$

is positive at the stimulus site. The right-hand side of Eq. (9) is defined to be the function $b(\mathrm{DI}_{S2},\mathrm{DI}_{S3},\mathrm{DI}_{S4})$, for use later.

Each of these equations has a similar physical interpretation, which we explain using Eq. (9) as an example. The first term on the right-hand side accounts for the difference in velocities between the S4 wavefront $v(\mathrm{DI}_{S4})$ and a hypothetical S5 wavefront that is launched so as to trail the S4 wave as closely as possible [that is, launched with $\mathrm{DI}=\mathrm{DI}_{\min}$ so that its velocity is $v(\mathrm{DI}_{\min})$]. If the trailing edge of the S4 wave were traveling at the same velocity $[v(\mathrm{DI}_{S4})]$ as its wavefront, it is clear intuitively that the S5 wave would immediately run into it if $v(\mathrm{DI}_{\min}) > v(\mathrm{DI}_{S4})$. This is consistent with the sign of this first term, which would be positive for this case, implying that block would occur, were it not for the presence of the remainder of terms on the right-hand side. The trailing edge of S4, does not, however, actually move with the same velocity as the leading edge, because of the variation of APD of the wave in space. This is just the effect accounted for by these remaining terms, which, from the derivation of Eq. (9), or through direct comparison of Eq. (9) with Eq. (4), are equal to $d\mathrm{APD}_{S4}/dx$. Furthermore, the form of these remaining terms shows that this gradient in APD results from the dynamics of previous waves, as characterized by their different propagation speeds and APD restitution slopes.

The blocking properties of waves generated by this stimulus protocol, as characterized by Eqs. (6)–(9), can be divided naturally into two categories, depending on whether the conduction is "normal" for all values of DI [i.e., $v'(\mathrm{DI}) \geq 0$ for all DI], or "supernormal" for some values of DI [i.e., $v'(\mathrm{DI}) < 0$ for some DIs]. In the case of normal conduction, we must always have $v(\mathrm{DI}_{\min}) \leq v(\mathrm{DI})$ for all other values of $\mathrm{DI} > \mathrm{DI}_{\min}$. This means that the first term on the right-hand side of Eqs. (6)–(9) is always negative or zero. Since there are no other terms on the right-hand side of Eq. (6), this implies that the S2 wave can never block under conditions of normal conduction. In the other equations, the remaining terms must create a positive spatial gradient in APD to create block.

The forms of Eqs. (7)–(9) thus suggest two kinds of patterns of stimulus intervals that tend to promote block in the case of normal conduction. Both patterns work by minimizing the magnitude of the negative first term on the right-hand side, while simultaneously making the remaining terms on the right-hand side as positive as possible. Again taking Eq. (9) as an example, the first pattern takes advantage of the fact that the last three terms are alternately added and subtracted. All three terms will then be positive if the CV of the last S1 wave $v(\mathrm{DI}_{SS})$, and the CVs of S2 through S4, alternate in magnitude so that the sign of the factor involving the CVs in each of these three terms also alternates. Specifically, all three terms will be positive if the S1S2, S2S3, and S3S4 stimulus intervals are chosen so that $\mathrm{DI}_{S2} < \mathrm{DI}_{SS}$, $\mathrm{DI}_{S3} > \mathrm{DI}_{S2}$ and $\mathrm{DI}_{S4} < \mathrm{DI}_{S3}$, assuming $a(\mathrm{DI})$ is a monotonically increasing function (which is typical). Choosing the S3S4 stimulus interval so that DI_{S4} is small also minimizes the magnitude of the first term. Assuming, as is typical, that the range of DI_{S}s for which block occurs is relatively small, this condition corresponds to the "short, long, short, short" pattern described previously [13], where "short" and "long" refer to the magnitude of the four diastolic intervals, DI_{S2} through DI_{S5}.

A second pattern of DIs that tends to yield type-II block during normal conduction takes advantage of the product of one or more factors of $a'(\mathrm{DI})$ that appears in each of the last three terms. These terms will tend to be larger in magnitude, therefore, if as many of DI_{S2}, DI_{S3} and DI_{S4} can be chosen to fall on the steepest part of APD restitution function as possible. In general, these two strategies cannot be optimized by the same set of DI_{S2}, DI_{S3}, and DI_{S4}; thus some compromise with respect to one or both strategies is needed to produce the highest likelihood of block.

The forms of Eqs. (6)–(9) allow us to make other observations. When the portion of the APD restitution function used has slope greater than 1, then the most important term in Eq. (9) is generally the last one, since it contains three factors of the slope. It is natural under these circumstances to think of the three slopes $a'(\mathrm{DI}_{S2})$, $a'(\mathrm{DI}_{S3})$, and $a'(\mathrm{DI}_{S4})$ as amplification factors, magnifying the disparity in inverse velocities associated with consecutive action potentials. The implication is that, when the slopes are greater than 1, the likelihood of block is substantially enhanced when multiple stimuli are applied, even if the initial disparity in conduction velocities between consecutive beats is small.

In contrast, when the APD restitution function slope is less than 1, the first two terms in Eq. (9) become the important terms. If block is to occur in this case, $v(\mathrm{DI}_{S4})$ should be as close to $v(\mathrm{DI}_{\min})$ as possible, and $a'(\mathrm{DI}_{S4})$ should be as large as possible. We also note that, when the APD restitution function slope is less than 1, it is just as feasible to try to create type-II block on the S3 action potential [see, Eq. (7)], in this case, choosing DI_{S2} carefully in analogous fashion. Both cases demonstrate that type-II block is possible even if the APD restitution function has slope less than 1, although perhaps less likely, since the process producing block is no longer helped by the amplification mechanism described above.

When the CV restitution function contains intervals of supernormal conduction [where $v'(\mathrm{DI})<0$], the situation is more complicated. In this case, $v(\mathrm{DI}_{\min})$ is no longer necessarily the smallest of all possible velocities. This makes it possible for the wavefront of a wave following just behind another [and thus moving at a velocity near $v(\mathrm{DI}_{\min})$] to be traveling faster than the wavefront of the wave it is trailing. This possibility is reflected in the first term on the right-hand sides of Eqs. (6)–(9), which now may be of either sign. We therefore observe that, when the wave in front is traveling slower than $v(\mathrm{DI}_{\min})$, the trailing wave will now crash into the wave it is following and block, unless dynamics creating the spatial gradient in APD *prevents* this collision. In particular, the S2 wave, whose governing equation (6) contains no dynamics associated with APD restitution, will always block if launched with a small enough DI, provided the velocity of the S1 wave $v(\mathrm{DI}_{SS})$ is slower than $v(\mathrm{DI}_{\min})$. Other terms on the right-hand sides of Eqs. (7)–(9) may also be opposite in sign from their counterparts during normal conduction, which then substantially changes the sets of S2–S5 intervals that cause type-II block. Since supernormal conduction is less common, we will not treat it further here, except to note that Eqs. (2)–(9) remain valid for this case, and thus can be used in its study.

V. COMPARISON TO A COUPLED MAP MODEL

A. The simulation model

To test the validity of the blocking condition, we compared the predictions described above to the pattern of blocks produced by the repeated running of a spatially one-dimensional coupled maps computer simulation. Four different APD restitution functions were combined with the same CV restitution function to form four "models" on which we conducted our tests. The CV restitution function in common to all four models was the one employed by Fox *et al.* [13], namely,

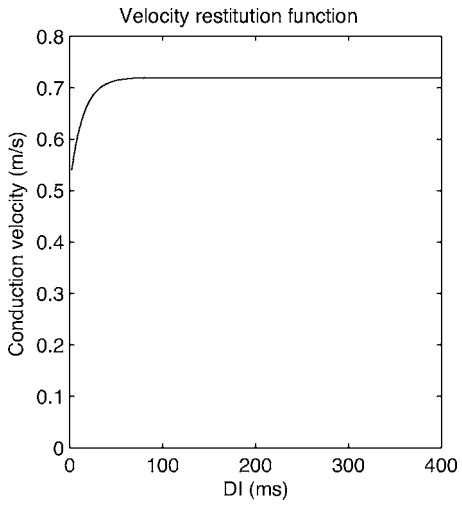

FIG. 8. Conduction velocity restitution function used in all four models.

$$v(\mathrm{DI}) = 0.72(1 - e^{-(\mathrm{DI}+17.408)/14.0}). \tag{10}$$

As shown in Fig. 8, the conduction is velocity is constant until the DI falls below about 50 ms where it decreases with decreasing DI.

Model No. 1 calculated APD restitution with the function

$$a(\mathrm{DI}) = 60 + \frac{150}{1 + e^{-(\mathrm{DI}-30)/28}}, \tag{11}$$

shown in Fig. 9(a). The slope of the function $a'(\mathrm{DI})$ is greater than 1 for $\mathrm{DI}<61$ ms, and flattens out for larger DI.

Model No. 2 employed an APD restitution function of the form

$$a(\mathrm{DI}) = 110 + \frac{100}{1 + e^{-(\mathrm{DI}-30)/28}}, \tag{12}$$

which has a slope less than 1 for all DI, as shown in Fig. 10(a).

The APD restitution function employed by model No. 3 took a different form

$$a(\mathrm{DI}) = \frac{f_1 e^{(\mathrm{DI}-52)/15} + f_2 e^{-(\mathrm{DI}-52)/15}}{e^{(\mathrm{DI}-52)/15} + e^{-(\mathrm{DI}-52)/15}}, \tag{13}$$

where

$$f_1 = 225 - 118e^{-\mathrm{DI}/115}, \tag{14}$$

$$f_2 = 92 + 10e^{(\mathrm{DI}-70)/40}. \tag{15}$$

As shown in Fig. 11(a), the function is steep over an intermediate range of DIs, with slope greater than 1 for 39 ms $<\mathrm{DI}<72$ ms, and is fairly flat near $\mathrm{DI}=0$.

Model No. 4 employed the same APD restitution function as that used by Fox *et al.* [13]; namely,

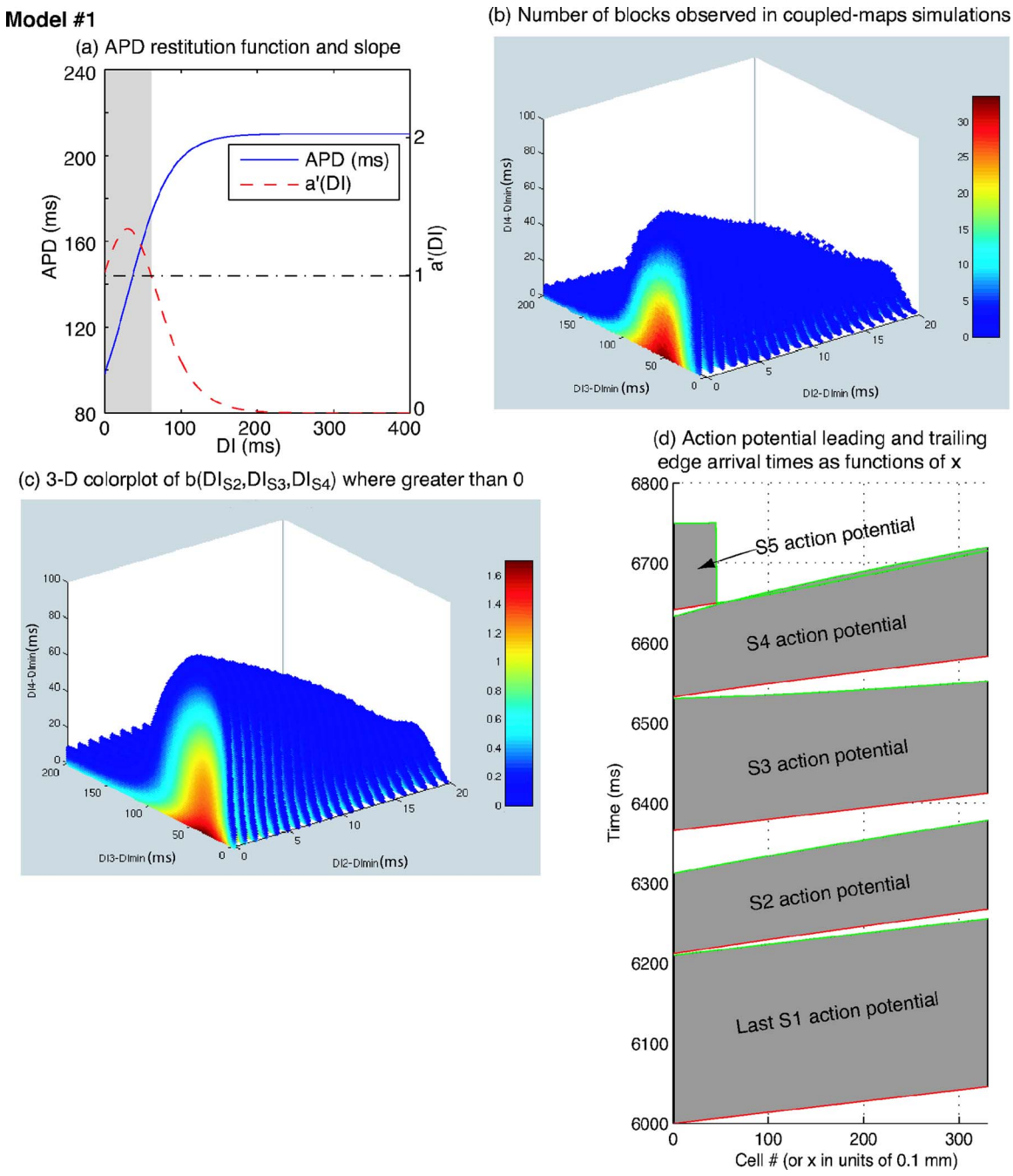

FIG. 9. (Color online) Model No. 1: (a) APD restitution function and its slope, $a'(\mathrm{DI})$. The slope is greater than 1 in the region shaded in gray ($0 \leq \mathrm{DI} < 61$ ms). (b) Colorplot of the number of type-II blocks of the S5 wave as a function of the values of DI_{S2}, DI_{S3} and DI_{S4} relative to $\mathrm{DI}_{\mathrm{min}}$ obtained from coupled-maps simulations of the Model No. 1 APD and CV restitution functions. (c) Values of $b(\mathrm{DI}_{S2}, \mathrm{DI}_{S3}, \mathrm{DI}_{S4})$, plotted only when positive as colored points, as functions of DI_{S2}, DI_{S3} and DI_{S4} (relative to $\mathrm{DI}_{\mathrm{min}}$). (d) Trajectories of the leading and trailing edges of the last S1 action potential wave, and the S2, S3, S4 and S5 action potential waves, for stimuli timed to yield the following DIs at the stimulus site: $\mathrm{DI}_{S2} = \mathrm{DI}_{\mathrm{min}}$, $\mathrm{DI}_{S3} = \mathrm{DI}_{\mathrm{min}} + 54$ ms, $\mathrm{DI}_{S4} = \mathrm{DI}_{\mathrm{min}}$, and $\mathrm{DI}_{S5} = \mathrm{DI}_{\mathrm{min}} + 4$ ms. The trajectories are shown as plots of the functions $t_d(x)$ and $t_r(x)$, the times of passage of the depolarizing and repolarizing edges of each wave, as functions of the location x.

$$a(\mathrm{DI}) = 88 + \frac{122}{1 + e^{-(\mathrm{DI}-40)/28}}, \tag{16}$$

as shown in Fig. 12(a). This allowed direct comparison with the default model appearing in Fox *et al.* [13].

The coupled maps simulations we used here were simplified versions of those employed by Fox *et al.* [13] in that they included no memory or electrotonic effects to create the simplest possible situation. The simulations consisted of a series of 330 "cells" arranged in a line. Dynamical variables for each cell j ($j = 0, 1, \ldots, 329$) were updated with the pas-

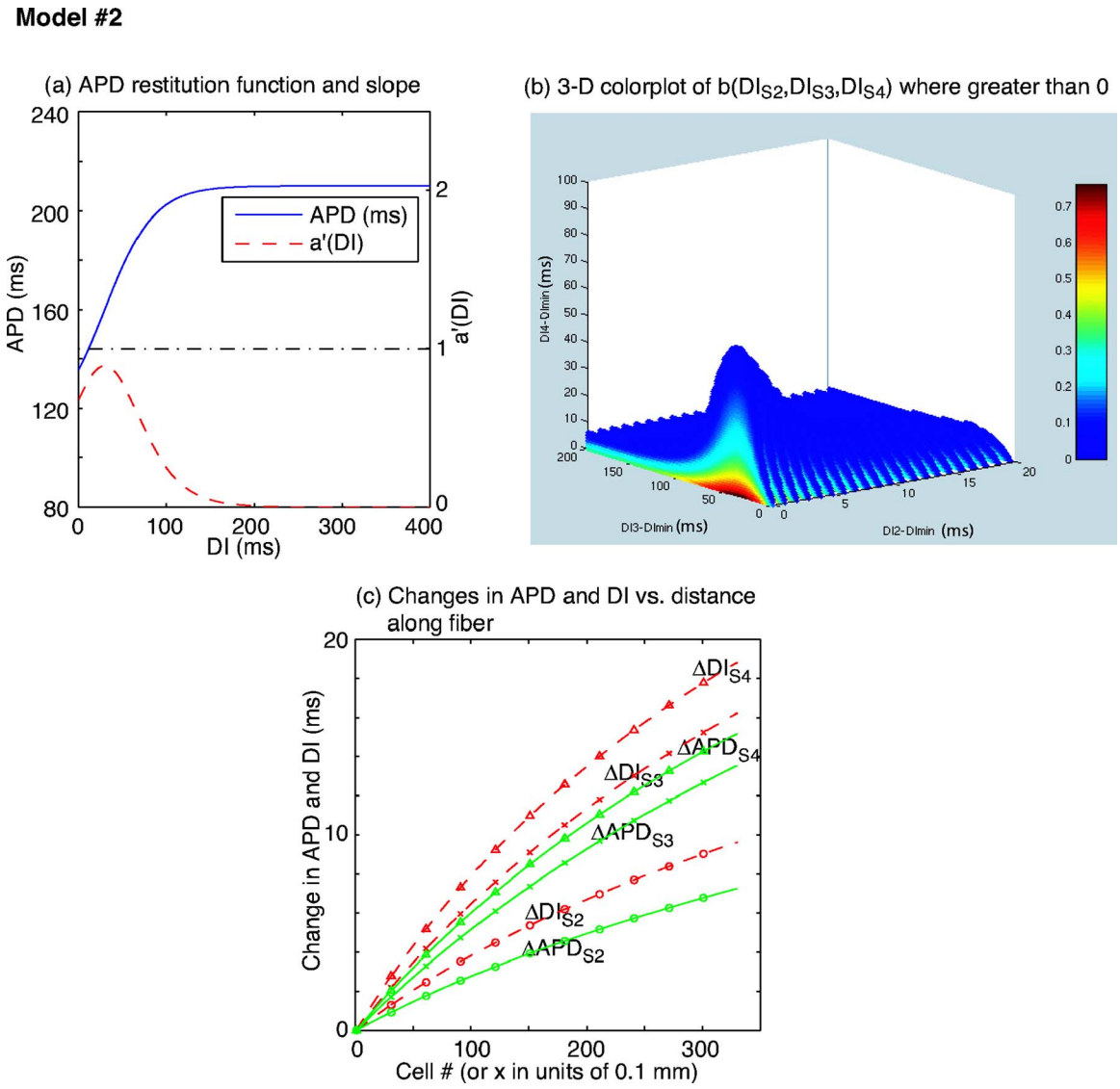

FIG. 10. (Color online) Model No. 2: (a) APD restitution function and its slope, $a'(\mathrm{DI})$. Note that the slope is always less than 1. (b) Values of $b(\mathrm{DI}_{S2},\mathrm{DI}_{S3},\mathrm{DI}_{S4})$, plotted only when positive as colored points, as functions of DI_{S2}, DI_{S3} and DI_{S4} (relative to $\mathrm{DI}_{\min}$). (c) $|\mathrm{DI}_{Si}(x)-\mathrm{DI}_{Si}(0)|$ (labeled $\Delta\mathrm{DI}_{Si}$) and $|\mathrm{APD}_{Si}(x)-\mathrm{APD}_{Si}(0)|$ (labeled $\Delta\mathrm{APD}_{Si}$) vs x for $i=2,3,4$, for stimuli chosen so that $\mathrm{DI}_{S2}=\mathrm{DI}_{\min}$, $\mathrm{DI}_{S3}=\mathrm{DI}_{\min}+50$ ms and $\mathrm{DI}_{S4}=\mathrm{DI}_{\min}+1$ ms. Circles, X's, and triangles denote quantities associated with stimuli 2, 3 and 4, respectively. The ΔDI quantities are shown as red, dashed lines; the ΔAPD quantities as green solid lines.

sage of each action potential wave as follows:

$$\mathrm{APD}_n(x_j) = a[\mathrm{DI}_{n-1}(x_j)], \tag{17}$$

$$\mathrm{CL}_n(x_j) = \mathrm{CL}_n(0) + \sum_{k=1}^{j-1} \Delta x/v[\mathrm{DI}_n(x_k)] - \sum_{k=1}^{j-1} \Delta x/v[\mathrm{DI}_{n-1}(x_k)], \tag{18}$$

$$\mathrm{DI}_n(x) = \mathrm{CL}_n(x) - \mathrm{APD}_n(x), \tag{19}$$

where $x_j=j\Delta x$ is the location of the jth cell, $\mathrm{CL}_n(x_j)$ is the time interval (the "cycle length") between the nth and $(n+1)$st action potential wavefronts at location x_j, and $\Delta x=0.1$ mm is the spacing between adjacent cells. The stimulus was applied in the 0th cell located at $x_0=0$. The two sums in Eq. (18) give the times required for the $(n+1)$st and nth wavefronts, respectively, to reach the cell located at x_{j-1}. These two times appear in the equation for CL_n because differences in CVs of the two wavefronts modify the cycle length as the two waves travel down the system. Equations (17)–(19) were evaluated one action potential at a time, starting with the cell at the stimulus location $x_0=0$ and proceeding away from the stimulus location: $x_1, x_2, \ldots$. The nth wave was assumed to block at a location x_j when $\mathrm{DI}_{n-1}(x_j)$ was found to be less than $\mathrm{DI}_{\min}$. $\mathrm{DI}_{\min}$ was chosen to be 2 ms to allow direct comparison to the results of Fox *et al.* [13].

All simulations were initialized with $\mathrm{DI}_0(x_j)=\overline{\mathrm{DI}}$, where $\overline{\mathrm{DI}}$ is the steady state value of DI when the cycle length $\mathrm{CL}=1000$ ms [i.e., $\overline{\mathrm{DI}}$ is the solution to $\overline{\mathrm{DI}}+a(\overline{\mathrm{DI}})=1000$]. The simulations were then paced for ten periods with a pacing interval of 500 ms. These ten stimuli are the S1 stimuli

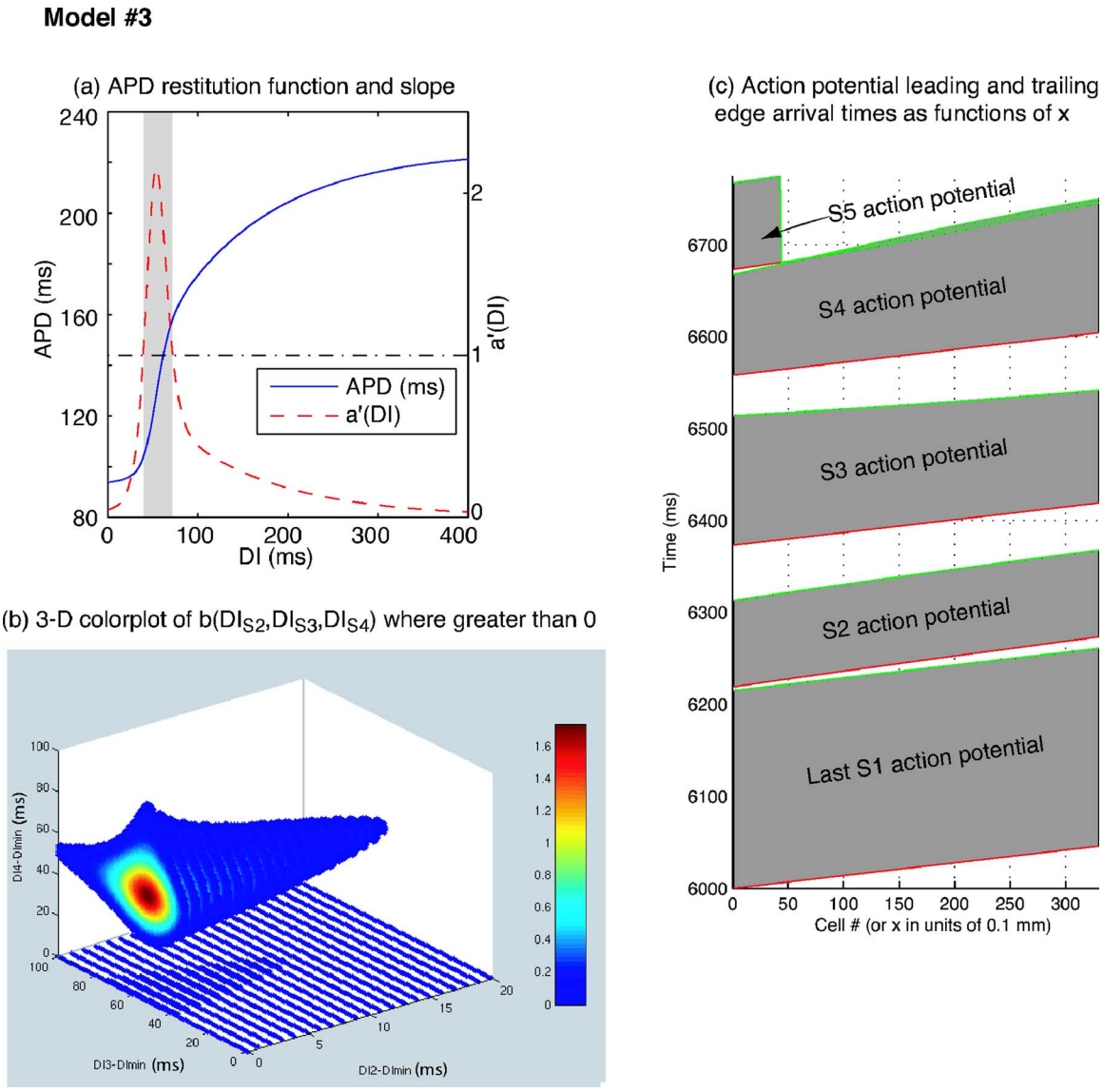

FIG. 11. (Color online) Model No. 3: (a) APD restitution function, designed to flatten out at short DIs. The slope of this function is greater than 1 in the gray region (39 ms $<$ DI $<$ 72 ms). (b) Values of $b(\mathrm{DI}_{S2},\mathrm{DI}_{S3},\mathrm{DI}_{S4})$, plotted only when positive as colored points, as functions of DI_{S2}, DI_{S3} and DI_{S4} (relative to $\mathrm{DI}_{\min}$). (c) Trajectories of the leading and trailing edges of the last S1 action potential wave and the S2, S3, S4 and S5 action potential waves, for stimuli timed to yield the following DIs at the stimulus site: $\mathrm{DI}_{S2}=\mathrm{DI}_{\min}+2$ ms, $\mathrm{DI}_{S3}=\mathrm{DI}_{\min}+58$ ms, $\mathrm{DI}_{S4}=\mathrm{DI}_{\min}+42$ ms, and $\mathrm{DI}_{S5}=\mathrm{DI}_{\min}+4$ ms. The trajectories are shown as plots of the functions $t_a(x)$ and $t_r(x)$, the times of passage of the depolarizing and repolarizing edges of each wave, as functions of the location x.

referred to earlier. Examination of action potential waves generated by the last two of these ten stimuli showed that the waves had settled down into the steady state associated with a pacing interval of 500 ms; i.e., $\mathrm{DI}(x)=\mathrm{DI}_{SS}$, $\mathrm{APD}(x)=a(\mathrm{DI}_{SS})$, and $v[\mathrm{DI}(x)]=v(\mathrm{DI}_{SS})$ independent of x and constant from one action potential to the next.

A search algorithm [20] was used to run the simulation repeatedly and report when blocks occurred. The algorithm ran a very large number of simulations (thousands) with different values of CL_{S2}, CL_{S3}, CL_{S4}, and CL_{S5}, where CL_{S2} is defined to be the time interval between the last S1 stimulus and the first premature stimulus S2 at the stimulus site, and the remaining CLs were defined consecutively (see Fig. 7). The algorithm included some "smart" features that allowed it to skip over large regions of $(\mathrm{CL}_{S2},\mathrm{CL}_{S3},\mathrm{CL}_{S4},\mathrm{CL}_{S5})$ space that were known not to contain type-II blocks. Details of the algorithm appear in the Appendix.

B. Results for model No. 1: Steep APD restitution

The quantity $b(\mathrm{DI}_{S2},\mathrm{DI}_{S3},\mathrm{DI}_{S4})$ appearing in Eq. (9) is a measure of the difference between the (inverse) velocity of the trailing edge of S4 and a hypothetical S5 wavefront following immediately behind it, with $\mathrm{DI}_{S5}=\mathrm{DI}_{\min}$. Since $b>0$ is a sufficient condition for the existence of a set of S5 waves that block, the set of $(\mathrm{DI}_{S2},\mathrm{DI}_{S3},\mathrm{DI}_{S4})$ combinations satisfying the condition $b>0$ should be a subset of those that produce type-II block in the coupled maps simulations. Furthermore, if situations of the type depicted in Fig. 5 do not occur, the two sets should be identical. We also observe that,

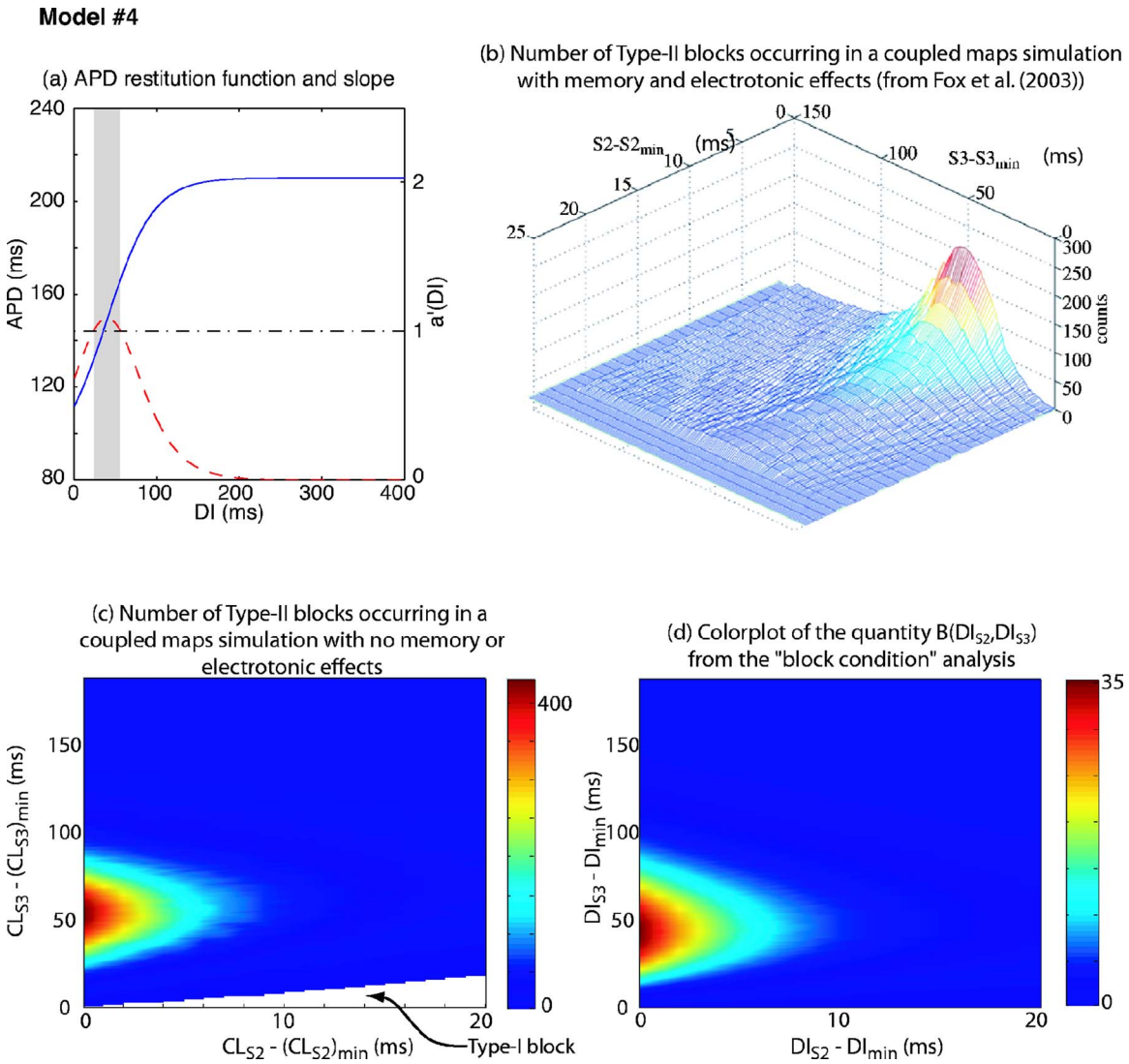

FIG. 12. (Color online) Model No. 4: (a) APD restitution function, also used in [13], and its slope, $a'(\mathrm{DI})$. The slope is greater than 1 in the gray-shaded region. (b) Number of type-II blocks for various combinations of CL_{S2} and CL_{S3} (referred to as S2 and S3, respectively, in the plot) produced by the coupled-maps simulations from the study of [13] (reproduced with permission). (c) Colorplot of the number of $(\mathrm{CL}_{S4},\mathrm{CL}_{S5})$ cycle length combinations that produced type-II action potential block in our coupled-maps simulations vs. the stimulus cycle lengths CL_{S2} and CL_{S3}. (See Appendix for detailed definitions.) Type-I block of the S3 wave occurs for the $(\mathrm{CL}_{S2},\mathrm{CL}_{S3})$ combinations located in the triangular white region at the bottom of the plot. (d) Colorplot of the quantity $B(\mathrm{DI}_{S2},\mathrm{DI}_{S3})$ vs. $\mathrm{DI}_{S2}-\mathrm{DI}_{\mathrm{min}}$ and $\mathrm{DI}_{S3}-\mathrm{DI}_{\mathrm{min}}$.

the more positive b is, the slower the trailing edge of S4 moves compared to the hypothetical S5 wavefront. This makes it easier for the S5 wave to catch up with and block on the S4 trailing edge. Consequently, we expect there to be a correlation between the magnitude of b, when positive, and the range of DI_{S5} values that cause type-II block of S5.

To test these assertions, we programmed our search algorithm to tabulate the total number of type-II blocks occurring in model No. 1 coupled-maps simulations for each combination of CL_{S2}, CL_{S3}, and CL_{S4} or, equivalently, for each combination of $(\mathrm{DI}_{S2},\mathrm{DI}_{S3},\mathrm{DI}_{S3})$ appearing at the stimulus site resulting from a given combination of $(\mathrm{CL}_{S2},\mathrm{CL}_{S3},\mathrm{CL}_{S4})$. The results appear in Fig. 9(b). The data are displayed as a large number of colored dots in three-dimensional parameter space—one for each combination of $(\mathrm{DI}_{S2},\mathrm{DI}_{S3},\mathrm{DI}_{S4})$ (relative to $\mathrm{DI}_{\mathrm{min}}$) that results in at least one instance of block. The color of each dot then indicates the number of blocks that occurred for that combination. We then plotted the values of $b(\mathrm{DI}_{S2},\mathrm{DI}_{S3},\mathrm{DI}_{S4})$, when positive, as colored dots in the same $(\mathrm{DI}_{S2},\mathrm{DI}_{S3},\mathrm{DI}_{S4})$ coordinate system, as shown in Fig. 9(c).

As expected, the shapes of the regions filled with colored dots are very similar in the two plots. In both plots, the filled region has a peak-like structure located in the same place in the three-dimensional $(\mathrm{DI}_{S2},\mathrm{DI}_{S3},\mathrm{DI}_{S4})$ volume. The widths of the peak-like structure are essentially the same in the two plots, with the half-width in the DI_{S2} direction, 8 ms, being much smaller than the half-widths in the other two directions

(40 ms). Additionally, the region containing the largest number of blocks per $(DI_{S2}, DI_{S3}, DI_{S4})$ combination [the red region in Fig. 9(b)] also approximately coincides with the region of maximum b [the red region in Fig. 9(c)], although the maximum occurs at slightly different points $(DI_{S2}, DI_{S3}, DI_{S4}) = DI_{min} + (0, 52, 0)$ ms in the former, vs. $DI_{min} + (0, 40, 0)$ ms in the latter. The discrepancy may be explained by noting that the magnitude of b is predicted to be correlated, but not necessarily functionally related, to the number of type-II blocks.

We note that the pattern of DIs that corresponds to the maximum in both plots is consistent with the form of Eq. (9); that is, the values of DI_{S2} through DI_{S5} follow the short-long-short-short pattern in both cases, as expected. This pattern is particularly effective in maximizing the quantity $b(DI_{S2}, DI_{S3}, DI_{S4})$, since the slope of the APD restitution function is greater than 1 over a large range of DIs [the gray region in Fig. 9(a)], including the entire range over which the CV restitution function varies (DI between 0 and about 40 ms). Thus, choices for $(DI_{S2}, DI_{S3}, DI_{S4})$ such as $DI_{min} + (0, 40, 0)$ ms or $DI_{min} + (0, 52, 0)$ ms yield large, positive values for all three slopes of relevance, $a'(DI_{S2})$, $a'(DI_{S3})$, and $a'(DI_{S4})$, and near maximally large changes in successive inverse velocities, $1/v(DI_{SS})$, $1/v(DI_{S2})$, $1/v(DI_{S3})$, and $1/v(DI_{S4})$. This minimizes the magnitude of the lone negative term in the expression appearing in Eq. (9) (the first term) and makes positive and maximizes the other three terms.

Examination of the trajectories of the last S1 wave and the S2 through S5 waves for a typical set of DI values taken from the peak region in Fig. 9(b) shows that the behavior of the individual propagating waves is as expected. As shown in Fig. 9(d), the small value of DI_{S2} at the stimulus site at $x = 0$ causes slow propagation of the leading edge of the S2 wave, which produces a widening gap between it and the trailing edge of the S1 wave as the S2 wave propagates left to right, thus creating a positive gradient in DI_{S2}. This gradient is amplified by the steep slope of the APD restitution curve, resulting in a longer S2 wave APD on the right side of the system than on the left. The trailing edge of the S2 wave thus travels even more slowly than the S2 leading edge. The large value of DI_{S3} creates a rapidly propagating S3 leading edge. The convergence of the S2 trailing edge with the S3 leading edge produces a large negative gradient in DI_{S3} in space.

We can also express the mechanism leading to this negative gradient in slightly different terms. The small value of DI_{S2} and large value of DI_{S3} produce, respectively, a slowly propagating S2 leading edge, and a rapidly propagating S3 leading edge. As a result, the time spacing between the two leading edges must be narrowing from left to right, although it is not particularly obvious in Fig. 9(d). This narrowing space is partially filled with the S2 action potential, which is widening from left to right, due to a positive gradient in DI_{S2} amplified by the steep slope in the restitution curve at small values of DI_{S2}. The two effects, the narrowing gap between the S2 and S3 leading edges caused by the difference in S2 and S3 leading edge propagation velocities, and the widening of the S2 action potential, cause the gap between the trailing edge of S2 and leading edge of S3 to narrow quite substantially from left to right, implying a strong negative gradient in DI_{S3}.

We observe that these two effects are exactly those expressed mathematically by Eq. (5) when $DI_n = DI_{S3}$. The equation shows that the gradient in DI_{S3} [i.e., the left-hand side of Eq. (5)] is affected by two quantities. The first is the difference in S2 and S3 leading edge inverse velocities, the first two terms on the right-hand side of Eq. (5), which will be nonzero anytime the S2 and S3 leading edge velocities are different. The second quantity is the third term on the right-hand side, which expresses the gradient in the S2 APD as $a'(DI_{S2})$, the slope of the APD restitution function at DI_{S2}, times the gradient in the previous DI, DI_{S2}.

This same mechanism, with all the polarities reversed, creates the widening of the gap between the S3 wave trailing edge and the S4 wave leading edge, corresponding to a positive spatial gradient in DI_{S4}. This gradient, in turn, is amplified by the steep slope of the APD restitution relation at short DIs such as DI_{S4} to produce a large positive gradient in the S4 APD. Finally, this positive APD gradient, combined with the slow propagation speed of the S4 leading edge, causes the trailing edge of the S4 wave to travel very slowly, allowing the S5 wave to catch up and crash into it. We note that the mechanism by which S5 type-II block occurs is that depicted in Fig. 4, and is thus the one assumed by our theory. Specifically, we observe that $dt_r^{S5}/dx < 1/v(DI_{min})$ for all values of x between 0 and the point at which block of the S5 wave occurs.

C. Results for model No. 2: Shallow APD restitution

Type-II block is still possible when the slope of the APD restitution curve is everywhere less than 1, as illustrated using model No. 2 [Fig. 10(a)]. As shown in Fig. 10(b), block is again predicted to occur when four premature stimuli are delivered so as to create a short-long-short-short pattern of DIs at the stimulus site. Application of the coupled-maps simulation to model No. 2 yields a pattern of block in $(DI_{S2}, DI_{S3}, DI_{S4})$ parameter space (not shown) as similar to Fig. 10(b) as Fig. 9(c) was to Fig. 9(b).

The mechanism by which block occurs may be explained through an examination of the gradients of the DIs and APDs of S2, S3 and S4 obtained from the coupled-maps simulation. We use the case of premature stimuli delivered with $DI_{S2} = DI_{min}$, $DI_{S3} = DI_{min} + 50$ ms, and $DI_{S4} = DI_{min}$ as an example. This combination of DIs falls in the red region in Fig. 10(b) and is thus a reasonable representative of the process by which block is created in model No. 2. In Fig. 10(c) are plotted DI_{S2}, APD_{S2}, DI_{S3}, APD_{S3}, DI_{S4}, and APD_{S4} as functions of x. Each of the quantities is plotted as the absolute value of its departure from its value at the stimulus site at $x = 0$, to simplify the comparison of their slopes. We observe that $|d\mathrm{APD}_i/dx| < |d\mathrm{DI}_i/dx|$ for each of the premature action potentials $i = 2, 3, 4$, as expected, since $a'(\mathrm{DI})$ is everywhere less than 1. Nevertheless, we still have $|d\mathrm{APD}_4/dx| > |d\mathrm{APD}_3/dx| > |d\mathrm{APD}_2/dx|$, owing to the fact that more terms involving differences between inverse conduction velocities appear in the expressions for $d\mathrm{APD}/dx$ for the later

action potentials. This additive effect is large enough to compensate for the fact that each of these differences is being multiplied by more and more factors of the APD restitution function slope, each of which is less than 1. The resulting value of $d\mathrm{APD}_4/dx$ slows down the trailing edge of the S4 wave below the critical velocity of $v(\mathrm{DI}_{\mathrm{min}})$, allowing the S5 wave to run into it and block. Block is in fact possible for this combination of $(\mathrm{DI}_{S2},\mathrm{DI}_{S3},\mathrm{DI}_{S4})$ for DI_{S5} as large as $\mathrm{DI}_{\mathrm{min}}+8$ ms.

D. Results from model No. 3: S-shaped APD restitution function

Our theory also shows that type-II block can occur with other patterns of DI_{S2} through DI_{S5} other than short-long-short-short. For example, if the APD restitution function is flattened at very short DIs, but steepened at intermediate DI, as in model No. 3 [Fig. 11(a)], we find that type-II blocking of the S5 wave occurs as depicted in Figs. 11(b) and 11(c). For this model, we again obtain reasonable agreement between the coupled-maps simulations (not shown) and the predictions based on the quantity $b(\mathrm{DI}_{S2},\mathrm{DI}_{S3},\mathrm{DI}_{S4})$ derived from the blocking condition [Fig. 11(b)]. We find that, in both cases, the conditions are most favorable for block when DI_{S3} and DI_{S4} are relatively large and DI_{S2} is near zero. Specifically, the maximum in the number of blocks seen in the simulations occurs at $(\mathrm{DI}_{S2},\mathrm{DI}_{S3},\mathrm{DI}_{S4})=\mathrm{DI}_{\mathrm{min}}+(0,59,42)$ ms, while the maximum in b occurs at $\mathrm{DI}_{\mathrm{min}}+(0,53,53)$ ms. Thus both cases suggest that a short-long-long-short pattern in DI_{S2} through DI_{S5} is most conducive to creating type-II block. The range of values of DI_{S3} and DI_{S4} defining the cylindrically shaped set of points exhibited in Fig. 11(b) substantially overlap the values of DI for which $a'(\mathrm{DI})>1$ $(39\ \mathrm{ms}<\mathrm{DI}<72\ \mathrm{ms})$, shown in gray in Fig. 11(a), facilitating the instances of block observed for combinations of DI_{S3} and DI_{S4} in this range.

We can obtain some understanding of why this pattern appears by careful examination of the S5 type-II blocking condition (9). One key lies in realizing the importance of the slope of the APD restitution curve at DI_{S4}. We observe that $a'(\mathrm{DI}_{S4})$ appears in all three of the terms that have the potential to cancel the negative first term on the right-hand side of Eq. (9). Thus, it is important that DI_{S4} be chosen so that $a'(\mathrm{DI}_{S4})$ is large and positive. For the model No. 3 APD restitution function, this occurs for DIs around 50 ms, near the middle of the $v'(\mathrm{DI})>1$ region shaded in gray [see Fig. 11(a)]. The steepness of the APD restitution function at this point is so important that it outweighs the fact that the first term in Eq. (9) is quite negative for this DI, owing to the associated fast CV, $v(50\ \mathrm{ms})$, compared to $v(\mathrm{DI}_{\mathrm{min}})$. The apparent necessity to choose DI_{S4} so that $v(\mathrm{DI}_{S4})$ is large also implies that the second term in Eq. (9) cannot help create block; it can only hurt. This is because the difference in inverse velocities in this term can, at best, be made only marginally negative, since $1/v(\mathrm{DI}_{S4})$ is so small. So, we choose DI_{S3} large enough so that $v(\mathrm{DI}_{S3})\approx v(\mathrm{DI}_{S4})$ to minimize the damage, and move on the third term. Here we find that choosing DI_{S2} small can really help to produce block, because then $v(\mathrm{DI}_{S2})$ is small and $v(\mathrm{DI}_{S3})$ is large, which makes the difference in inverse velocities in the third term large and positive. Furthermore, if we choose DI_{S3} so that it also falls in the steep part of the APD restitution curve, we can make the amplifying factor $a'(\mathrm{DI}_{S3})$ as large as $a'(\mathrm{DI}_{S4})$, resulting in a very large and positive third term. Of course, choosing DI_{S2} small also implies that the fourth term will be relatively inconsequential, because the APD restitution function is flat at small DI, and thus $a'(\mathrm{DI}_{S2})$ is small. Thus, we see that the main contributor to producing type-II block in model No. 3 is the third term in Eq. (9).

We can see this block mechanism at work in Fig. 11(c). Since the APD restitution function is flat at short DIs, such as DI_{S2}, the S2 APD is roughly constant in x, despite the fact that a gradient in DI_{S2} exists. The leading and trailing edges of the S2 wave therefore travel at approximately the same velocity. A spatial gradient in DI_{S3} is therefore created by the long DI_{S3} since it causes the S3 leading edge to move faster than the leading and therefore the trailing edge of the S2 wave. We then observe that this gradient in DI_{S3} is amplified by $a'(\mathrm{DI}_{S3})$, creating larger gradients of the S3 APD and DI_{S4}. The gradient in DI_{S4} is then amplified again by $a'(\mathrm{DI}_{S4})$, creating an even larger gradient in the APD of S4. We see that, even though this gradient is being added to the relatively fast-moving leading edge of the S4 wave, the result is a slow enough moving S4 trailing edge that the S5 action potential can run into it, creating type-II block. Again, we observe that block is occurring via the mechanism depicted in Fig. 4.

E. Results from model No. 4: Comparison to Fox *et al.*

Finally, we checked to see whether our theory was consistent with the simulation results obtained by Fox *et al.* [13]. Accordingly, we defined the APD and CV restitution functions of model No. 4 to be exactly those used by Fox *et al.* [13] for their default case. We also programmed the search algorithm to tabulate the total number of type-II blocks that were found in coupled-maps simulations of model No. 4 for each $(\mathrm{CL}_{S2},\mathrm{CL}_{S3})$ pair (rather than each $\mathrm{CL}_{S2},\mathrm{CL}_{S3},\mathrm{CL}_{S4}$ combination) to allow direct comparison with similarly presented data in their paper. The results of this tabulation are shown in Fig. 12(c).

To allow direct comparison to the predictions of the blocking condition, we summed positive values of b over DI_{S4} to yield a quantity that only depends on the S2 and S3 stimulus timings

$$B(\mathrm{DI}_{S2},\mathrm{DI}_{S3}) \equiv \sum_{\mathrm{DI}_{S4}=\mathrm{DI}_{\mathrm{min}}}^{\mathrm{DI}_{\mathrm{min}}+100\ \mathrm{ms}} b(\mathrm{DI}_{S2},\mathrm{DI}_{S3},\mathrm{DI}_{S4}) \times H[b(\mathrm{DI}_{S2},\mathrm{DI}_{S3},\mathrm{DI}_{S4})], \tag{20}$$

where $H(\xi)$ is the Heaviside function, defined to be 1 if $\xi>0$ and 0 otherwise. The upper bound of the sum was chosen large enough to comfortably include all likely blocks for all combinations of DI_{S2} and DI_{S3} examined. When B was evaluated for all combinations of DI_{S2} between $\mathrm{DI}_{\mathrm{min}}$ and $\mathrm{DI}_{\mathrm{min}}+20$ ms and DI_{S3} between $\mathrm{DI}_{\mathrm{min}}$ and $\mathrm{DI}_{\mathrm{min}}+185$ ms, we obtained the colorplot shown in Fig. 12(d).

To compare the results displayed by the two plots in Figs. 12(c) and 12(d), we note the left edges of the two plots correspond to one another, since in both cases, type-I block of the S2 stimulus occurs to the left of these edges, given that $CL_{S2} < (CL_{S2})_{min}$ and $DI_{S2} < DI_{min}$ both by definition cause type-I block. Also, the upper boundary of the type-I block region of Fig. 12(c) corresponds to the bottom edge of Fig. 12(d) (where $DI_{S3} = DI_{min}$), since again both define the boundary below which type-I block of the S3 stimulus occurs.

Comparison of Figs. 12(b)–12(d) shows that the distribution of type-II blocks yielded by our simulations and those of Fox *et al.* [13] agree reasonably well with the shape of the function $B(DI_{S2}, DI_{S3})$. The maximum number of blocks occurred at $(DI_{S2}, DI_{S3}) = DI_{min} + (0, 50)$ ms in the simulations of Fox *et al.* and at $DI_{min} + (0, 57)$ ms in our coupled maps simulations, while the peak in the function $B(DI_{S2}, DI_{S3})$ occurred at $(DI_{S2}, DI_{S3}) = DI_{min} + (0, 42)$ ms. The widths of the peak in all three cases are comparable, being approximately 8 ms in the DI_{S2} direction, and 35 ms in the DI_{S3} direction in each case. The slight disparities obtained might be accounted for by the fact that Fox *et al.*'s simulations include memory and electrotonic effects, whereas ours do not, and by the fact that the quantity B is expected to be correlated, but again not strictly functionally related to the number of type-II blocks.

VI. INCLUSION OF MEMORY

It is widely recognized that the APD does not depend just on the previous DI but also on other quantities that, in turn, are determined by other aspects of the previous history of the cells. Thus, it is important to extend our theory to incorporate the effects of the other quantities, collectively often called "memory," into the APD restitution dynamics. Here, we take a first step into examining the effects of memory by deriving the basic equations and considering the quantity analogous to $a'(\mathrm{DI})$, the APD restitution function slope. Inclusion of memory typically results in equations of the form (e.g., Otani and Gilmour [21]),

$$\mathrm{APD}_n = a(\mathrm{DI}_{n-1}, \mathbf{M}_n), \tag{21}$$

where $\mathbf{M}$ is a vector of memory dynamical variables whose dynamics is determined by

$$\mathbf{M}_{n+1} = \mathbf{m}(\mathbf{M}_n, \mathrm{APD}_n, \mathrm{DI}_n) \tag{22}$$

and a and $\mathbf{m}$ are the generalized APD restitution function and a "memory" function, respectively. Other slightly different forms of these equations are possible; for example, see Cain *et al.* [17].

We can construct the equation analogous to Eq. (5) by subtracting $1/v[\mathrm{DI}_n(x)]$ from both sides of Eq. (2), substituting Eq. (3), and differentiating Eqs. (21) and (22) with respect to x. We obtain,

$$\frac{d\mathrm{DI}_n}{dx}(x) = \frac{1}{v[\mathrm{DI}_n(x)]} - \frac{1}{v[\mathrm{DI}_{n-1}(x)]} - \frac{d\mathrm{APD}_n}{dx}(x), \tag{23}$$

$$\frac{d\mathbf{M}_{n+1}}{dx}(x) = \frac{\partial \mathbf{m}}{\partial \mathbf{M}}\frac{d\mathbf{M}_n}{dx} + \frac{\partial \mathbf{m}}{\partial \mathrm{APD}}\frac{d\mathrm{APD}_n}{dx} + \frac{\partial \mathbf{m}}{\partial \mathrm{DI}}\frac{d\mathrm{DI}_n}{dx}, \tag{24}$$

$$\frac{d\mathrm{APD}_n}{dx} = \frac{\partial a}{\partial \mathrm{DI}}\frac{d\mathrm{DI}_{n-1}}{dx} + \frac{\partial a}{\partial \mathbf{M}}\frac{d\mathbf{M}_n}{dx}, \tag{25}$$

where the derivatives of $\mathbf{m}$ are evaluated at $[\mathbf{M}_n(x), \mathrm{APD}_n(x), \mathrm{DI}_n(x)]$ and the derivatives of a are evaluated at $[\mathrm{DI}_{n-1}(x), \mathbf{M}_n(x)]$. By substituting Eq. (25) into Eqs. (23) and (24) and Eq. (23) into Eq. (24), we find that Eqs. (23) and (24) may be written as

$$\begin{bmatrix} \frac{d\mathrm{DI}_n}{dx} \\ \frac{d\mathbf{M}_{n+1}}{dx} \end{bmatrix} = \left(\frac{1}{v[\mathrm{DI}_n(x)]} - \frac{1}{v[\mathrm{DI}_{n-1}(x)]} \right) \begin{bmatrix} 1 \\ \frac{\partial \mathbf{m}}{\partial \mathrm{DI}} \end{bmatrix} - \mathsf{A} \cdot \begin{bmatrix} \frac{d\mathrm{DI}_{n-1}}{dx} \\ \frac{d\mathbf{M}_n}{dx} \end{bmatrix}, \tag{26}$$

where A is a square matrix whose elements are algebraic combinations of the derivatives of the functions a and $\mathbf{m}$ appearing in Eqs. (23) and (25).

We observe that repeated iteration of Eq. (26) leads to an equation analogous to Eq. (9), with A playing the role of a'. In turn, we observe that A is the linear operator that determines how perturbations in $(\mathrm{DI}_n, \mathbf{M}_{n+1})$ propagate from one beat to the next under the constraint of constant cycle length. [This can be seen by noting that A respects the relationship $d(\mathrm{DI}_n + \mathrm{APD}_n)/dx = 0$ from Eq. (23).] Thus, we can anticipate that the amplification produced by repeated application of A may be most closely tied to the dynamic stability of APDs under conditions of constant pacing, even though A is not being evaluated at steady-state values for $(\mathrm{DI}, \mathbf{M})$, which would technically be necessary for the comparison to be rigorous.

We also note that the quantities contained in the vector $\mathbf{M}$ need not be memory quantities as normally defined; the derivation is sufficiently general that $\mathbf{M}$ may be any set of dynamical variables, for example, gating variables, ionic concentrations and/or the membrane potential at some specified time, that, along with DI, determine the next values of themselves and the next DI. Thus, to the extent that such a system can be constructed, it is more generally true that the dynamical stability of perturbations under situations of constant pacing including, in particular, alternans, is closely related to the likelihood of type-II block, through the stability of the matrix A, evaluated for the values of $(\mathrm{DI}, \mathbf{M})$ associated with each action potential generated at the stimulus site.

VII. DISCUSSION AND SUMMARY

In this paper, we have derived a mathematical condition that will guarantee that an action potential wave, launched from one end of a spatially one-dimensional system, will

block at some nonzero distance away from the stimulus site. The condition, that $dt_r/dx > 1/v(\mathrm{DI}_{\mathrm{min}})$ at the stimulus site, simply says that block at-a-distance, also called type-II block, will occur if the velocity of the trailing edge of the previous wave is smaller, when evaluated at the stimulus site, than the velocity at which waves travel when the preceding DI is the smallest for which propagation is possible $[v(\mathrm{DI}_{\mathrm{min}})]$. This condition, which we call the "blocking condition," is valid with only relatively modest restrictions: (1) the conduction velocity must be solely a function of the preceding diastolic interval [i.e., $v=v(\mathrm{DI})$], (2) propagation failure occurs below a well-defined diastolic interval $\mathrm{DI}_{\mathrm{min}}$, and (3) the velocity of the trailing edge of the preceding wave must be a continuous function of x.

These restrictions guarantee that leading edge trajectories cannot cross, which allows us to construct a topological argument for why the blocking condition must result in type-II block (see Fig. 4). In turn, the topological nature of this condition provides it with a measure of robustness—that is, the condition remains valid under a variety of improvements of the underlying model. In particular, the inclusion of memory and electrotonic effects in the determination of the APD, as defined in Echebarria and Karma [6], have no effect on the validity of the blocking condition. Electrotonic effects modifying the leading edge will affect the condition, however, since then the leading edge velocity depends on the states of nearby cells, and so is no longer solely a function of the previous DI. While the condition is fairly general, we reiterate that it is only a sufficient condition for type-II block; type-II block can occur through mechanisms other than the one we concentrate on here.

To study some of the consequences of the blocking condition, we evaluated it for a case of interest—that of a small number of premature (i.e., short cycle length) stimuli being applied to a system that has settled down to a steady state following a series of stimuli applied with a constant, longer cycle length. The form of the blocking condition (9) reveals a clear mechanism for type-II block for this case. Type-II block tends to occur when differences in the CVs between pairs of consecutive waves are amplified sufficiently by steep slopes of the APD restitution function to slow the trailing edge of one of the waves so that the following wave can collide with it. Thus, block at-a-distance is most likely to occur when the inter-stimulus intervals are chosen to maximize (1) the difference in CVs of each consecutive pair of waves and (2) the slopes of the APD restitution function at each DI interval. The ideal situation is for the set of DIs corresponding to the steepest part of the APD restitution curve to include a complete range of available CVs. It is then possible to choose a series of DIs from within this range that yields a set of maximal consecutive CV differences, each of which is then amplified one or more times by the steep part of the APD restitution curve. This situation was essentially the case illustrated by model No. 1. More generally, however, some compromise must be made in the choices of DI so as to hit the steep part of the APD restitution curve as often as possible, while still generating as many large velocity differences as possible, as was the case in model No. 3.

It is not too difficult to see why this kind of prescription works. Under normal circumstances [i.e., in the absence of supernormal conduction, when $v'(\mathrm{DI})<0$], the velocity of the leading edge following a DI equal to $\mathrm{DI}_{\mathrm{min}}$ is slower than the velocity following any other propagating value of DI. Therefore, to satisfy the blocking condition, a positive spatial gradient in APD must be established to slow the velocity of the trailing edge relative to the leading edge. This APD gradient may be generated by first creating a gradient in DI by launching two successive waves with different leading edge velocities. (Before the APD gradient is generated, the trailing edge velocity of the first wave is equal to its leading edge velocity. The difference between this velocity and the leading edge velocity of the second wave then creates the gradient in DI.) This DI gradient appears in the following APD gradient in amplified form, with amplification provided by the steepness in the APD restitution curve. A negative version of this APD gradient is then transferred to the next DI gradient, to which is added any new DI gradient produced by the difference in the next leading edge velocity and the previous one. This process of repeated amplification by steep APD restitution and addition of new velocity differences continues until the APD gradient is large enough to make the trailing edge of the corresponding wave slow enough to allow the blocking condition to be satisfied, permitting the next wave, if launched with small enough DI, to "run into" the preceding trailing edge.

It is interesting that the slope of the APD restitution curve, which plays a central role in determining whether cells undergoing constant pacing exhibit alternans, also plays an important role here. As discussed in the Introduction, the susceptibility of cardiac tissue to alternans is also thought to render it vulnerable to action potential block, allowing possible subsequent development of spiral waves, spiral wave breakup and fibrillation. Although there is obviously a connection between the two types of dynamics, we note that there are also important differences. First, the appearance of the APD restitution curve slope does not arise from the consideration of linear (that is, small) perturbations around a steady state as it does in the theory of alternans. Our theory is fully nonlinear in this respect—it remains valid for large perturbations in the pacing cycle length and diastolic interval. Second, there exists a critical slope for APD restitution function in the theory of alternans. When the slope equals or exceeds 1, sustained alternans becomes possible. In our theory of type-II block, 1 is still an important number, since any time a DI is chosen so that the APD restitution slope exceeds this number, amplification of all the existing differences in velocities occurs. However, it is not essential that the slope be greater than 1—as we have seen from our study of model No. 2, if the differences between pairs of consecutive velocities are large enough, and the leading edge velocity of the last propagating wave is close enough to $v(\mathrm{DI}_{\mathrm{min}})$, type-II block on the next wave is still possible, even if the slope is less than 1. It is also possible for type-II block to not exist even though the slope of the APD restitution function exceeds 1. The obvious example is when $v(\mathrm{DI})$ is constant so that differences in velocities cannot be created.

Similar statements may be made when memory is present. In the theory of alternans, a matrix relates perturbations about a steady state from one stimulus to the next. We find that the same matrix is involved in the amplification process

that leads to type-II block. However, again, it is clear that the presence of eigenvalues that are larger than 1 in absolute value, which signals the onset of alternans in the case of constant pacing, does not necessarily mean that type-II block is possible. We also note that this matrix is not evaluated at steady state values in our theory, as it is in linear alternans theory.

Although an APD restitution slope greater than 1 (or a stability matrix with eigenvalues greater than 1 in absolute value) is neither necessary nor sufficient for type-II block to occur, it does in some sense increase the probability that block will occur, since repeated amplification of critical quantities leading to block is now possible. Accordingly, the appearance of alternans could serve as a diagnostic signal telling us that the tissue is more likely to be susceptible to type-II block. Thus, to the extent that type-II block may be related to clinically significant arrhythmias, the presence of alternans may be useful in alerting caregivers that conditions are favorable for the development of those arrhythmias.

ACKNOWLEDGMENTS

The author gratefully acknowledges useful discussions with R. F. Gilmour, Jr., A. Gelzer, and M. L. Riccio.

APPENDIX: ALGORITHM USED TO SEARCH FOR TYPE-II BLOCK

The search algorithm used to look for type-II blocks was designed so as to skip over combinations of CL_{S2} through CL_{S5} that are known not to produce block. The upper limits of these cycle lengths were also chosen in a judicious manner designed to capture all the "interesting" type-II block behavior. Specifically, the algorithm ran simulations for values of CL_{S2} between the smallest value that did not produce immediate block of the S2 wave at the stimulus site (called type-I block), and a value 20 ms longer, in 1 ms increments. For each of these values of CL_{S2}, the algorithm looked for type-II block of S3, starting with the smallest value of CL_{S3} that did not produce type-I block of S3, and increasing in 1 ms increments. This algorithm considered a block to be of type II if the wave was able to travel more than 0.1 mm (1 cell) before blocking, and type-I otherwise. Once S3 waves were able to travel across the system without type-II block, the algorithm continued to increase CL_{S3} in 1 ms steps, looking for type-II blocks of S4 and S5. The increments continued until either no type-II blocks of S4 or S5 were found and CL_{S3} had already been increased 70 ms, or until CL_{S3} reached 300 ms. To find these S4 and S5 type-II blocks, the algorithm applied the same procedure to CL_{S4}, as was just described for CL_{S3}: The algorithms searched for type-II blocks of S4 starting with the smallest value of CL_{S4} that did not result in type-I block of S4 with subsequent increments in 1 ms steps until type-II block of S4 no longer occurred. The algorithm then continued to increment CL_{S4}, looking for S5 type-II blocks, ending its search when either $CL_{S4}=400$ ms, or after CL_{S4} was 50 ms larger than its first value for this (CL_{S2},CL_{S3}) combination. Finally, the algorithm searched for the aforementioned type-II blocks of S5 by starting with the minimum value of CL_{S5} that did not produce type-I block, and continuing until the S5 wave propagated across the system.

The precise definitions of the quantities appearing in Fig. 12(c) were based on the code's operation: $(CL_{S2})_{min}$ is smallest value of CL_{S2} that does not cause the wave generated by S2 to exhibit type-I block, given that the preceding cycle length is the steady state cycle length, 500 ms, and $(CL_{S3})_{min}$ is defined as smallest value of CL_{S3} that does not cause type-I block of the S3 wave, given that the preceding cycle length is $(CL_{S2})_{min}$. The precise definition of the number of blocks for a given pair of cycles lengths CL_{S2} and CL_{S3} appearing in Fig. 12(c) is given as: the number of combinations of CL_{S4} and CL_{S5} that yield type-II block of the S5 wave, plus the number of values of CL_{S4} that cause the S4 wave to exhibit type-II block, plus 1, if the S3 wave terminates in a type-II block.

[1] F. X. Witkowski, L. J. Leon, P. A. Penkoske, W. R. Giles, M. L. Spano, W. L. Ditto, and A. T. Winfree, Nature (London) **392**, 78 (1998).
[2] P. S. Chen, P. D. Wolf, E. G. Dixon, N. D. Danieley, D. W. Frazier, W. M. Smith, and R. E. Ideker, Circ. Res. **62**, 1191 (1988).
[3] J. J. Fox, M. L. Riccio, F. Hua, E. Bodenschatz, and R. F. Gilmour, Jr., Circ. Res. **90**, 289 (2002).
[4] J. M. Pastore, S. D. Girouard, K. R. Laurita, F. D. Akar, and D. S. Rosenbaum, Circulation **99**, 1385 (1999).
[5] M. A. Watanabe, F. H. Fenton, S. J. Evans, H. M. Hasting, and A. Karma, J. Cardiovasc. Electrophysiol. **12**, 196 (2001).
[6] B. Echebarria and A. Karma, Phys. Rev. Lett. **88**, 208101 (2002).
[7] J. B. Nolasco and R. W. Dahlen, J. Appl. Physiol. **25**, 191 (1968).
[8] M. R. Guevara, G. Ward, A. Shrier, and L. Glass, Comput. Cardiol. **11**, 167 (1984).
[9] A. Karma, Chaos **4**, 461 (1994).
[10] A. Garfinkel, Y. H. Kim, O. Voroshilovsky, Z. Qu, J. R. Kil, M. H. Lee, H. S. Karagueuzian, J. N. Weiss, and P. S. Chen, Proc. Natl. Acad. Sci. U.S.A. **97**, 6061 (2000).
[11] R. H. Clayton and P. Taggart, Biomed. Eng. Online **4**, 54 (2005).
[12] E. M. Cherry and F. H. Fenton, Am. J. Physiol. Heart Circ. Physiol. **286**, 2332 (2003).
[13] J. J. Fox, M. L. Riccio, P. Drury, A. Werthman, and R. F. Gilmour, Jr., New J. Phys. **5**, 101.1 (2003).
[14] F. H. Fenton, E. M. Cherry, H. M. Hastings, and S. J. Evans, Chaos **12**, 852 (2002).
[15] M. Courtemanche, L. Glass, and J. P. Keener, Phys. Rev. Lett. **70**, 2182 (1993).
[16] J. J. Fox, R. F. Gilmour, Jr., and E. Bodenschatz, Phys. Rev.

Lett. **89**, 198101 (2002).
[17] J. W. Cain, E. G. Tolkacheva, D. G. Schaeffer, and D. J. Gauthier, Phys. Rev. E **70**, 061906 (2004).
[18] Z. Qu, A. Garfinkel, P.-S. Chen, and J. N. Weiss, Circulation **102**, 1664 (2000).
[19] P. Comtois, A. Vinet, and S. Nattel, Phys. Rev. E **72**, 031919 (2005).
[20] G. Buzzard (private communication).
[21] N. F. Otani and R. F. Gilmour, Jr., J. Theor. Biol. **187**, 409 (1997).